Ammonia Synthesis on the RRuSi(001) (R = Ca,La) Surfaces: DFT Insights Revealing the Active La Termination of the LaRuSi Electride

Florian Brix, Gilles Frapper, Émilie Gaudry

Ammonia Synthesis on the RRuSi(001) (R = Ca,La) Surfaces: DFT Insights Revealing the Active La Termination of the LaRuSi Electride

Florian Brix, Gilles Frapper, and Émilie Gaudry*

ABSTRACT: Recently, transition metal electrides have attracted the attention of scientists as promising catalysts for ammonia synthesis. But very little is known about the atomic processes involved. In this work, extensive DFT calculations have been performed to explore the detailed mechanism of ammonia synthesis on LaRuSi, a typical electride catalyst. Unlike previous studies involving the LaRuSi(001) high energy Ru-terminated surface, we propose here an alternative reaction path at the most stable La termination. Our study addresses the contrasted catalytic properties of the isostructural LaRuSi electride and CaRuSi non-electride compounds. It points to the role of surface La atoms in the catalytic performances of LaRuSi and shows that active sites are not necessarily transition metal atoms. Our findings open up future explorations of transition metal free catalysts for ammonia synthesis, active under mild conditions.

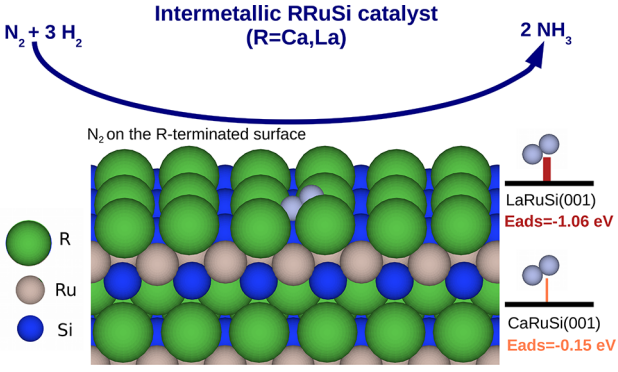

INTRODUCTION

Large scale production of ammonia, achieved through the Haber−Bosch process,[1,2] has deeply influenced our society through the synthesis of ammonia-based fertilizers.[3,4] Nowadays, ammonia is also envisioned to impact the forthcoming years in the context of the hydrogen economy. This is attributed to its high hydrogen content (3 kWh kg^{-1}) and gravimetric energy (17.7 wt %), which makes it an attractive hydrogen carrier and a "zero-carbon" fuel, releasing energy without CO_x emission.[5,6]

The formation of NH_3 from hydrogen and nitrogen is exothermic:[7,8] $\Delta H_f\left(\frac{3}{2}H_2 + \frac{1}{2}N_2 \rightarrow NH_3\right) = -45.5$ kJ mol^{-1}. However, to be kinetically feasible, efficient catalysts are required to cleave the strong N≡N bond, which is the rate limiting step in most cases.[9,10] Among the pure metals, ruthenium and osmium are recognized as the best catalysts,[11] while iron-based compounds are widely used in industry.[12] Electron donors, such as alkali metals, can promote the dissociation of N≡N, through electron transfer to the π^* antibonding orbitals of N_2.[13,14] Within this scheme, the Cs−Ru/MgO is nowadays one of the best industrial catalytic systems, even if it is easily prone to hydrogen poisoning[15,16] and requires harsh conditions, i.e., high temperatures (>400 °C) and pressures (>25 bar).[12,17]

New strategies are required to achieve ammonia synthesis under milder conditions. Besides photocatalytic and electrolytic approaches,[18−22] the engineering of strong metal−support chemical interactions, such as those between Ru and a nitride-based support (like $Ca(NH_2)_2$), can manage a high catalytic performance even at 473 K under ambient pressure.[23] Here, the key ingredients for the catalytic properties are (i) the combination of Ru with electropositive metals and (ii) the high hydrogen solubility of the support. Within this approach, several Ru-based intermetallic catalysts have been developed: YRu_2,[24] Ru/LaScSi,[25] Ru/C12A7e$^-$,[13] Ru/$RH_{3-2x}O_x$ (R = La, Ce),[26] Ru/LnRuSi (Ln = La, Ce, Pr),[27] etc. Among them, ternary electrides, i.e., inorganic ternary compounds with excess electrons located at given crystallographic sites that resemble anions,[28] have shown excellent catalytic activities.[25,27,29−31] Their good performances are attributed to their strong electron-donating effect to enhance the N_2 cleavage.[27,32] Depending on the relative values of the N_2 adsorption energy and the N_2 dissociation barrier, the reaction may proceed through a *hot atom* mechanism,[29] in which the energy released in the adsorption process is used to elevate the N_2 molecule's vibrational energy level and thus promote the bond breaking.[33−35]

For now, the proposed mechanism for ammonia synthesis catalyzed by ternary transition metal electrides relies on transition-metal-terminated surfaces.[27,29,30,36] However, the contrasting synthesis rates[30] over the LaRuSi and CaRuSi

Received: October 5, 2021
Revised: January 21, 2022

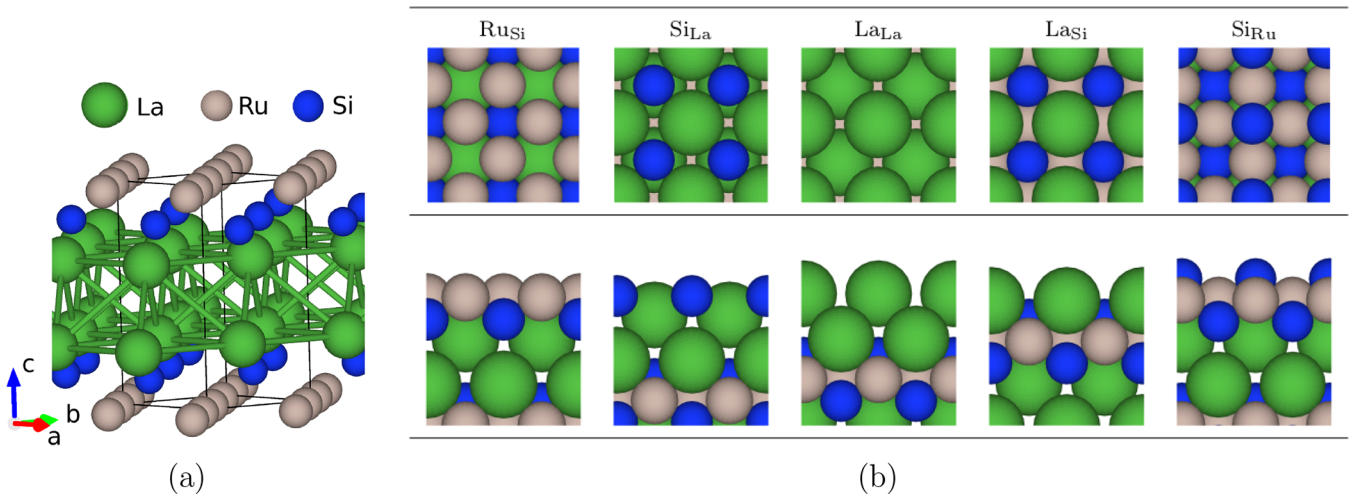

Figure 1. (a) Bulk structure of LaRuSi. The tetragonal crystal cell is shown in black. (b) Surface models (top and side views) for LaRuSi(001) resulting from a bulk truncation.

compounds are hardly compatible with this hypothesis. Indeed, the similar surface electronic structure of the two (001) terminations, with comparable charges carried by surface Ru atoms (−0.87 and −0.96 *e* for LaRuSi and CaRuSi, respectively),[37] is expected to lead to comparable catalytic properties. In addition, the lower surface energies of hcp La and fcc Ca than that of hcp Ru ($\gamma^{La}_{(0001)}$ = 0.70 J/m^2, $\gamma^{Ca}_{(111)}$ = 0.46 J/m^2, $\gamma^{Ru}_{(0001)}$ = 2.60 J/m^2),[38] suggest that La- and Ca-terminated surfaces are the most plausible ones. So far, no mechanism at the atomic scale for the ammonia synthesis has been proposed on a transition metal free termination. In this paper, using plane-wave density functional theory (DFT) calculations performed at $P = 0$ and $T = 0$, we propose a novel mechanism for the hydrogenation of N_2 to NH_3 on LaRuSi(001), based on extensive calculations of surface (γ), adsorption (E_{ads}), reaction (ΔE), and activation (E_{act}) energies. The activation barrier for N_2 dissociation (0.84 eV) is found to be much lower than the one on the Ru-terminated LaRuSi(001) surface (1.30 eV).[27] Moreover, we extend our DFT investigation on CaRuSi(001)—CaRuSi formally presents one less electron per formula unit than LaRuSi—to evaluate the impact of the electronic structure (electride character) on the nitrogen hydrogenation process.

COMPUTATIONAL METHODS

All calculations have been performed on the basis of the Density Functional Theory using the Vienna ab initio simulation package (VASP) .[39−41] The interactions between the valence electrons and the ionic core have been described using the spin polarized projector-augmented wave (PAW) method[42,43] within the DFT-D3 scheme,[44] considering the valences for the atoms to be $5s^25p^65d^16s^2$ (La), $4s^23p^6$ (Ca), $4p^65s^14d^7$ (Ru), $3s^23p^2$ (Si), $1s^1$ (H), and $2s^22p^3$ (N). The one-electron Kohn−Sham orbitals have been expanded with a kinetic energy cutoff of 450 eV. The reciprocal space integration has been approximated with a Monkhorst−Pack k-point grid of 4 × 4 × 4 and 4× 4 × 1 for the bulk and RRuSi(001) surfaces, respectively (R = Ca, La). Electronic structure and Bader charge[45−47] analyses have been performed using an increased energy cutoff (520 eV) and a finer *k*-point mesh (9 × 9 × 1).

This computational setup leads to lattice parameters in good agreement with experimental ones (Table S1). Surfaces have been modeled with 2 × 2 symmetric 6, 7, 8, and 10 layer thick slabs separated by a 20 Å void thickness. Structures have been relaxed until the forces dropped below 0.01 eV/Å. Surface energies have been computed as a function of the La and Si chemical potentials:

$$2\gamma A = E_{slab} - N_{La}\mu_{La} - N_{Si}\mu_{Si} - N_{Ru}\mu_{Ru} \quad (1)$$

where E_{slab}, N_i, and μ_i are the total energy of the slab and the number and the chemical potentials of atoms of type *i* in the slab, respectively.

Adsorption energies have been calculated using

$$E_{ads} = E_{adsorbate+slab} - E_{adsorbate} - E_{slab} \quad (2)$$

where $E_{adsorbate+slab}$, E_{slab}, and $E_{adsorbate}$ are the total energy of the {slab+adsorbate} system, of the slab, and of the free adsorbate, respectively.

Energy barriers have been determined on the basis of the climbing image nudged elastic band (CI-NEB) and dimer methods.[48−52] Seven intermediate images have been produced by linear interpolations between relaxed images. The optimization process was stopped when the change in the total (free) energy was smaller than 10^{-4} eV. Vibrational analysis (for saddle point verification), limited to the surface species and keeping the rest of the system fixed, has been carried out by calculating the Hessian matrix with a finite difference approach (step size of 0.015 Å). The dimer method[53] improved by Heyden et al.[52] has been used when more than one imaginary frequency was found.

Electronic structure analysis has been performed using Bader charges,[47,54,55] density of states, and projected Crystal Orbital Hamilton Population (pCOHP) methods.[56−59]

RESULTS AND DISCUSSION

Surface Structures. The crystal structure of RRuSi (R = La,Ca) is a tetragonal CeFeSi-type structure (*P*4/*nmm* space group, Figure 1a), made of (001) planes of edge-sharing $[R]_4$ tetrahedra alternating with layers built with Ru and Si atoms (sequence $Ru_{0.00}$-$Si_{0.17}La_{0.32}La_{0.68}Si_{0.83}Ru_{1.00}$ in the crystal cell where the subscript indicates the reduced z-ccordinate). In LaRuSi, the $[La]_4$ cavities show a localized electron charge

density (Figures S1a and S2a). Thus, LaRuSi is identified as an electride compound. In contrast, the $[Ca]_4$ interstitial sites do not contain any localized electron charges: CaRuSi does not belong to the family of electride compounds (Figures S1c and S2b). Interestingly, the tetrahedral $[R]_4$ sites can accept hydrogen atoms to form RRuSiH. In LaRuSi, it strongly modifies the electronic structure, since sites filled with atomic hydrogen no longer present an electride character (Figure S1b).[30]

From the sequence of (001) atomic planes in the bulk compound, five possible terminations (X_Y where X and Y stand for the compositions of the topmost and subsurface planes, respectively) can be built by bulk truncation: R_{Si}, Si_{Ru}, Ru_{Si}, Si_R, and R_R. The investigation of possible surface restructuring that could occur under real conditions is beyond the scope of this work. Surface energy calculations confirmed that the La_{Si} termination is the most stable one (0.74 J/m^2, Figure 2, Table S2), except in a small region in the vicinity of $\mu_{Si} = \mu_{Si}^{bulk}$ and $\mu_{La} = \mu_{La}^{bulk} + \Delta H_f$. Owing to its large domain of stability, we used the R-terminated (R_{Si}) surface model in the following. The low atomic density of the R termination leads to a non-negligible surface corrugation and implies that topmost Si atoms are exposed at the surface as well, in the 4-fold hollow sites made of four R atoms (Figure 1b). Since ammonia synthesis is known to be structure sensitive (highly active sites are the B5 and C7 sites on Ru(0001) and Fe(111), respectively[2,60−64]), such a corrugated structure likely favors the reaction. Transition metal atoms are located in the subsubsurface plane and are therefore hardly available to form bonds with adsorbates. The charges carried by topmost La, Si, and Ru (1.26 *e*, −0.30 *e*, and −0.90 *e*, respectively) are found in good agreement with the ones calculated by Wu et al. (1.16 *e*, −0.29 *e*, and −0.87 *e*). They are similar for LaRuSi(001) and CaRuSi(001) and are not impacted by the presence of hydrogen atoms in the underlying $[R_4]$ sites (Table S3). Nevertheless, the partial electron densities are larger at the LaRuSi(001) surface than at the CaRuSi(001) one (Figure S3). This is attributed to the different natures of La and Ca atoms (3 and 2 valence electrons, respectively).

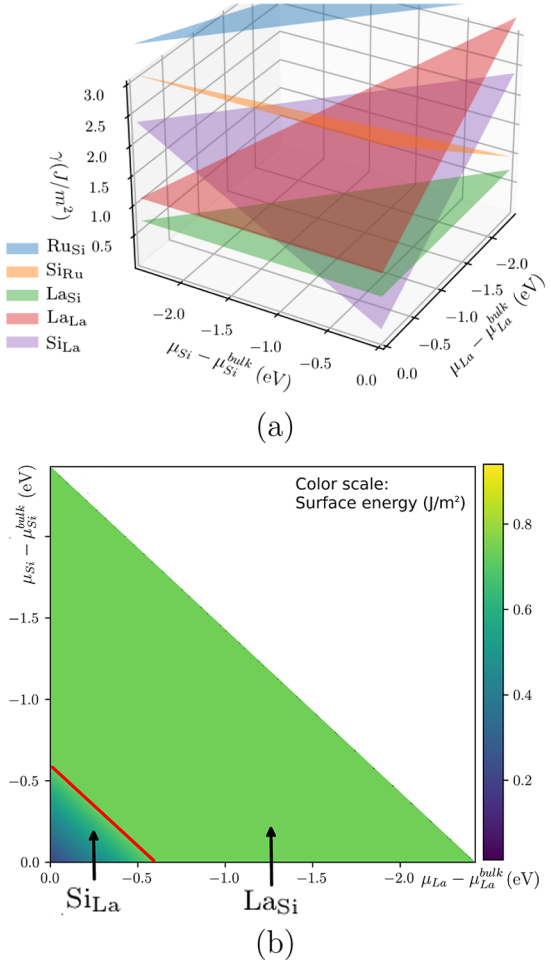

Figure 2. (a) Surface energies of surface models presented in Figure 1b, as a function of the Si and La chemical potentials. (b) Stability domains of most stable structures (Si_{La} and La_{Si}), resulting from surface energy minimization. The color scale represents the surface energies in J/m^2, and the red line is used to separate the regions where the Si_{La} and La_{Si} models are the most stable ones.

Dissociation of H_2. We now turn to the investigation of nitrogen hydrogenation to ammonia, using the R-terminated RRuSi(001) surface models. Hydrogenation reactions require the dissociation of H_2. The molecule is adsorbed in bridge sites (Tables S4−S6), between two surface R atoms, parallel to the surface and, thus, positioned above a subsubsurface Ru atom. It is highly activated: the H−H distance is 1.78 Å (R = La) and 1.09 Å (R = Ca). The H_2 molecule is more activated on La-terminated surfaces, in agreement with the larger electron transfer from the surface to the adsorbed molecule on LaRuSi(001) than on CaRuSi(001) (Figure S3). The larger filling of the H_2 antibonding σ^* orbitals leads to a larger H−H distance. The adsorption energy is rather low (E_{ads}^{LaRuSi} = −0.18 eV, E_{ads}^{CaRuSi} = −0.13 eV). The cleavage of the molecule is not spontaneous, in contrast to what happen on Ru[65] or La,[66] but occurs with a small activation energy (E_{act}^{LaRuSi} = 0.37 eV, E_{act}^{CaRuSi} = 0.31 eV, Table 1, Figure 3, Figure S4). Therefore, atomic hydrogen adsorbates may be abundant and available for nitrogen hydrogenation. The reaction energy of the hydrogen dissociation is smaller on RRuSi (ΔE^{LaRuSi} = −0.35 eV, ΔE^{CaRuSi} = −0.53 eV) than on Ru (ΔE^{Ru} = −0.91 eV)[65] or La (ΔE^{La} = −1.38 eV).[66] Once dissociated, the two hydrogen atoms diffuse to the neighboring Si top sites, with adsorption energies similar to the ones calculated on Ru (E_{ads}^{LaRuSi} = −2.51 eV, E_{ads}^{CaRuSi} = −2.64 eV, E_{ads}^{Ru} = −2.96 eV,[67] Figure 4). Hydrogen adatoms are bound to the surface Si site through covalent single bonds. But the Si−H distances are larger on RRuSi(001) (1.68 Å (R = La) and 1.64 Å (R = Ca)) than in crystalline SiH_4 (1.49 Å).[68]

N_2 Activation and Cleavage. Ammonia synthesis also requires the activation of the N_2 molecule. Nitrogen is adsorbed vertically, and slightly tilted, in a top Si site (Tables S4−S6). Although the adsorption geometries are rather similar on LaRuSi and CaRuSi, the adsorption energies considerably differ (Figure 4). Indeed, N_2 interacts weakly with the CaRuSi surface (E_{ads}^{CaRuSi} = −0.15 eV) but is strongly bound on LaRuSi (E_{ads}^{LaRuSi} = −1.06 eV). This is consistent with the strong adsorption of N_2 on lanthanide stepped (111) facets.[69] The stronger interaction between N_2 and LaRuSi(001) is clearly evidenced by the pCOHP calculations (Figure 5). The R−N integrated pCOHPs (ICOHPs, Table S7) are much smaller for R = Ca (−0.48 eV) than for R = La (−2.62 eV). That said, the Si−N ICOHPs are of the same order of magnitude for the two ternary compounds (−4.28 and −4.46 eV for CaRuSi and LaRuSi, respectively).

Table 1. Activation Energies (Reaction Energies in Parentheses) of the Elemental Steps for Ammonia Synthesis (Energies in eV)[a]

		LaRuSi	CaRuSi	$LaRuSiH_{1/2}$	$CaRuSiH_{1/2}$	Ru
$H_2 \rightarrow 2\ H$	TS1	0.37 (−0.35)	0.31 (−0.53)	0.40 (−0.24)	0.24 (−0.72)	
$N_2 \rightarrow 2\ N$	TS2	0.84 (−1.86)	0.87 (−1.64)	0.82 (−1.83)	1.00 (−1.83)	1.9,[72] 1.15,[73] 1.57 (−1.59)[74]
$N + H \rightarrow NH$	TS3	1.10 (−0.02)	1.34 (−0.52)	1.00 (−0.18)	1.33 (−0.39)	1.27 (0.07)[74]
$NH + H \rightarrow NH_2$	TS4	0.87 (0.22)	1.80 (0.34)	0.79 (0.11)	1.80 (0.50)	1.35 (0.50)[74]
$NH_2 + H \rightarrow NH_3$	TS5	0.86 (0.49)	1.27 (0.32)	0.74 (0.51)	1.32 (0.47)	(0.10)[74]

[a]The numbering of transition states are reported in Figures 3, 6, and 7.

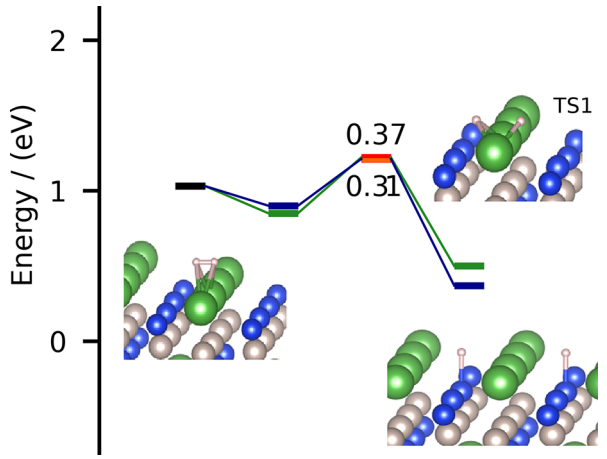

Figure 3. Reaction energy diagram for the H_2 dissociation on RRuSi(001) surfaces, with R = La (in green) and R = Ca (in blue). Transition state energies are plotted in orange (R = La) and red (R = Ca). The corresponding activation energies are given in eV. Optimized atomic configurations are shown in each case.

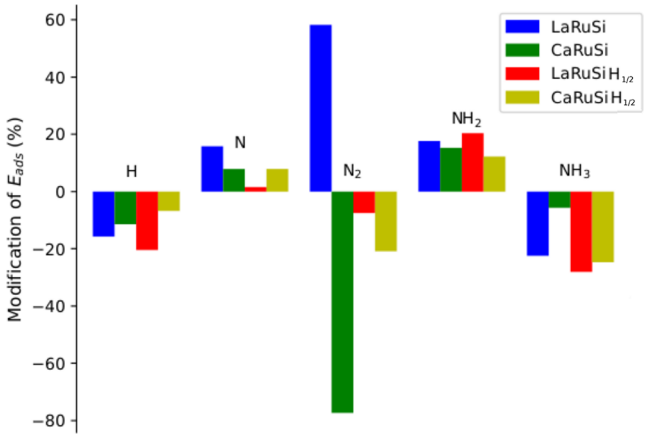

Figure 4. Adsorption energies of H, N, N_2, NH_2, NH_3 on RRuSi and $RRuSiH_{1/2}$ (partially hydrogenated compound) in comparison to the ones on Ru(0001). The modification of the adsorption energy is given by $\frac{E_{ads}^{X} - E_{ads}^{Ru}}{E_{ads}^{Ru}}$ with X ∈ {LaRuSi, CaRuSi, $LaRuSiH_{1/2}$, $CaRuSi_{1/2}$}.

The pCOHP analysis also points toward a N−N bond more activated on the LaRuSi surface than on the CaRuSi one. The bonding contributions of the nitrogen σ and π orbitals, located around −11 and −6 eV (Figure 5), are quite similar for the two compounds. In contrast, the π^* antibonding orbitals are more filled for N_2 on LaRuSi(001) than on CaRuSi(001). The charge donation from R to N_2 is actually larger for R = La than for R = Ca, in agreement with the larger electron charge density on LaRuSi(001) than on CaRuSi(001) (Figure S3).

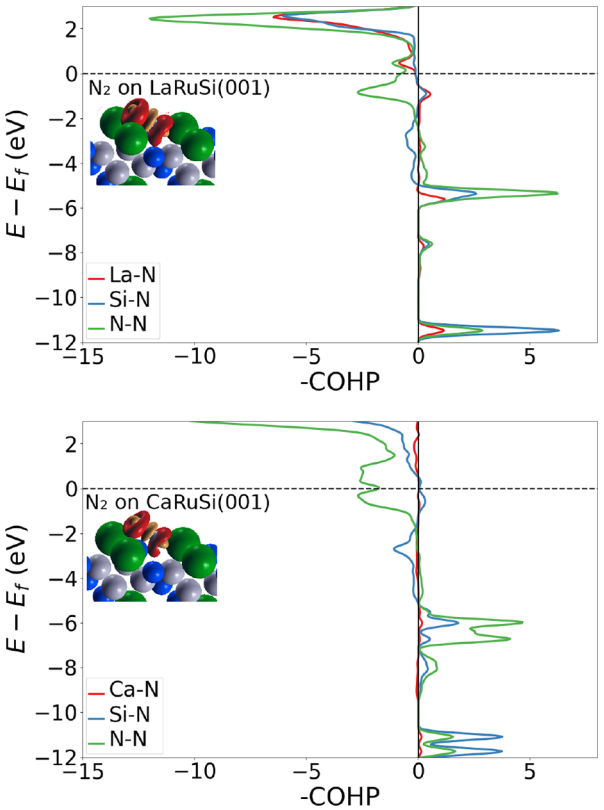

Figure 5. pCOHP analysis for N_2 adsorbed on the RRuSi(001) surface (R = Ca,La). Contributions of the R−N, Si−N, and N−N bonds to the COHPs are plotted in red, blue, and green, respectively. The charge deformation (isosurface, 0.07 $e/Å^3$) is plotted in each case.

This leads to a N−N chemical bond for adsorbed N_2, which is shorter and stronger on CaRuSi (1.26 Å, ICOHPs = −11.80 eV) than on LaRuSi (1.39 Å, ICOHPs = −9.04 eV).

Theoretical studies have predicted that good catalysts for ammonia synthesis bind N_2 with adsorption energies between −2 and −1 eV.[70,71] This is ensured here for LaRuSi, but not for CaRuSi, suggesting that such a descriptor may be relevant to identify efficient catalysis for ammonia synthesis. Interestingly, nitrogen adsorption on the Ru termination is much larger ($E_{ads}^{LaRuSi(Ru)}$ = −4.12 eV) and outside the predicted range.

Although LaRuSi and CaRuSi are quite different toward nitrogen adsorption, the calculated nitrogen dissociation barriers are similar on both catalysts (E_{act}^{LaRuSi} = 0.84 eV, E_{act}^{CaRuSi} = 0.87 eV, Table 1, Figure 6, Figure S5) and much lower than the one calculated on the LaRuSi Ru-terminated surface (1.30 eV).[27] This is in agreement with the apparent activation energies observed for the isotopic N_2 exchange (E_{act}^{LaRuSi} = 1.62

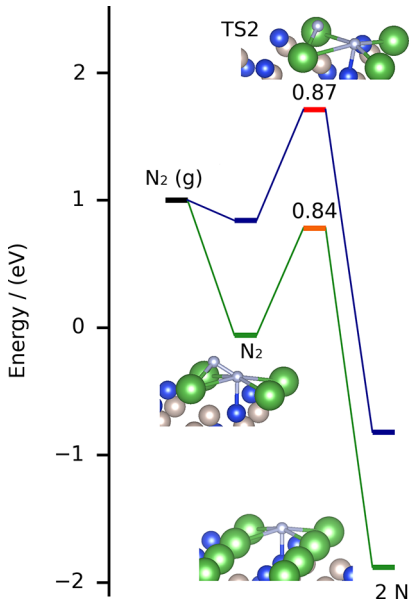

Figure 6. Reaction energy diagram for N_2 dissociation on RRuSi(001) surfaces, with R = La (in green) and R = Ca (in blue). Energies of transition states are plotted in orange (R = La) and red (R = Ca). The corresponding activation energies are given in eV. Optimized atomic configurations are shown in each case.

eV and E_{act}^{CaRuSi} = 1.76 eV eV for LaRuSi and CaRuSi, respectively).

The main driving force for the dissociation likely lies in the charge transfer, during the reaction, from the R-terminated catalyst's surface (R = Ca, La) to the N_2 molecule, that progressively fills the π^* antibonding orbitals. Indeed, the Bader charges on atomic nitrogen increase from −0.83 e (N_2 adsorbed on top Si site) to −1.52 e (transition state) on LaRuSi(001). The values are found similar at the CaRuSi(001) surface (−0.58 e and −1.47 e, respectively).

The main difference between the two catalysts, which may explain the contrasted behaviors of the CaRuSi and LaRuSi catalysts, is related to the relative values of the N_2 adsorption energies and dissociation barriers, evaluated through $\Sigma E = E_{ads} + E_{act}$. We found ΣE^{LaRuSi} = −0.18 eV and ΣE^{CaRuSi} = 0.72 eV. Thus, while the energy released in the adsorption process on LaRuSi is larger than what is needed to break the N_2 molecule (the energy released can promote the bond breaking), an amount of 0.72 eV is required to cleave the N_2 molecule on CaRuSi. Another limitation of the weak adsorption of N_2 on CaRuSi lies in the fact that the molecule likely desorbs when the temperature is high enough.

Nitrogen Hydrogenation to NH_3. Nitrogen dissociation requires a non-negligible activation energy on LaRuSi and CaRuSi. This energy is, however, much smaller than the barriers leading to the hydrogenated NH−NH and NH_2−N intermediates (2.40 and 2.79 eV, respectively, on LaRuSi). As a consequence, the associative mechanism, which has been explicitly considered on flat Ru or metal nitride surfaces[75,76] can be ruled out. Within the dissociative mechanism, the hydrogenation barriers of N+ H → NH, NH + H → NH_2, and NH_2 + H → NH_3 are 1.10 eV, 0.87 eV, and 0.86 eV on LaRuSi(001). They are much larger on CaRuSi(001) (1.34 eV, 1.80 eV, and 1.27 eV; see Table 1, Figure 7, Figures S6−S8). On LaRuSi, the formation of NH from atomic N and H proceeds with the highest barrier, while it is the hydrogenation of NH to NH_2 on CaRuSi.

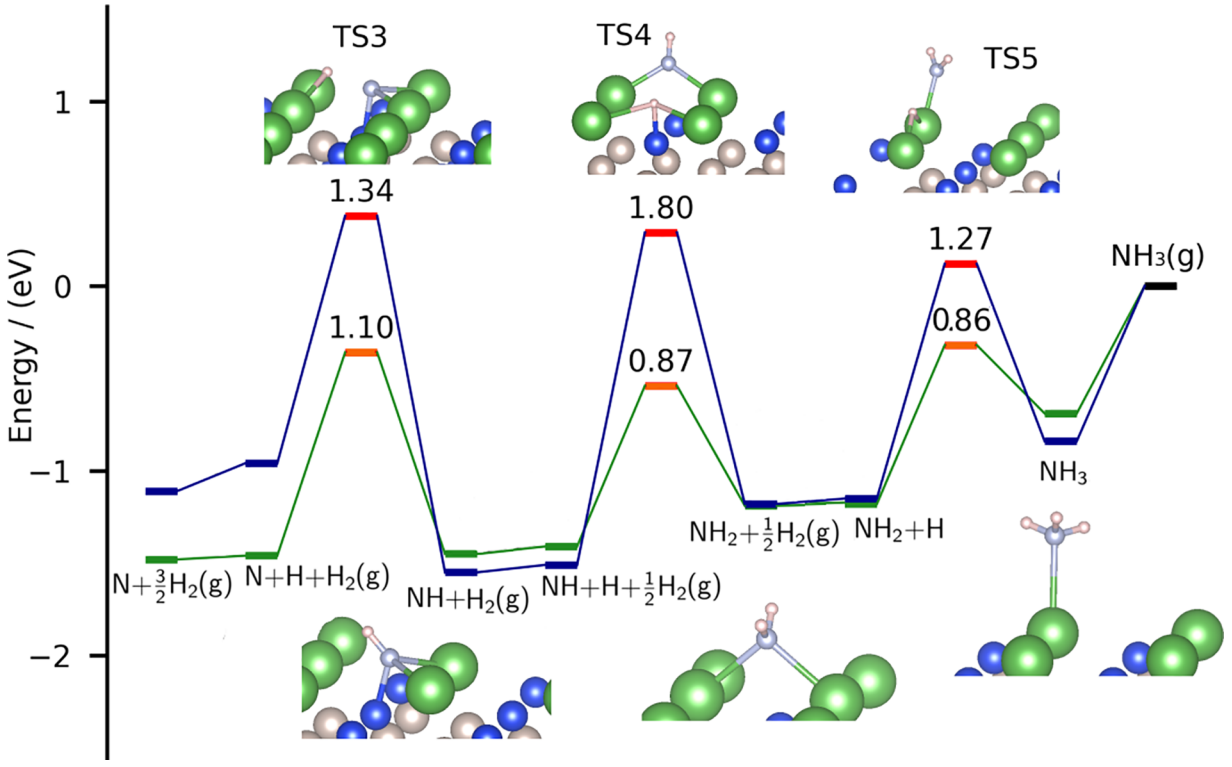

Figure 7. Reaction energy diagram for nitrogen hydrogenation on RRuSi(001) surfaces, with R = La (in green) and R = Ca (in blue). Transition state energies are plotted in orange (R = La) and red (R = Ca). The corresponding activation energies are given in eV. Optimized atomic configurations are shown in each case. All species are adsorbed, except for specified gas phase molecules.

The adsorption energies and the activation barriers of the reaction intermediates are not affected by hydrogen absorption (Table 1). Since the electride character disappears when the bulk $[R]_4$ sites are occupied by hydrogen atoms (Figure S1b), it suggests that the electride character does not impact the catalytic properties of the surface. This is in agreement with the high reaction rate even when the electride is converted completely to hydride,[16] which is likely, since hydrogen absorption is exothermic, stronger than adsorption ($E_H^{surf} - E_H^{bulk} = 0.25$ eV), and occurs with a barrier of the same order of magnitude as the hydrogenation steps (0.91 eV, for the diffusion from the surface to the bulk, Figure S9). Interestingly, other relevant hydrogenation catalysts are identified as compounds that can form hydrides, like $BaGa_2$ or Pd (ref 77 and references therein).

CONCLUSION

A detailed mechanistic investigation of ammonia synthesis on LaRuSi has been carried out. Surface energies and mechanistic calculations identify the La_{Si} termination as an active surface for the nitrogen reduction reaction to NH_3 and address the contrasted catalytic properties of LaRuSi and CaRuSi.

Adsorption properties of the R-terminated RRuSi(001) surfaces share similarities with the ones of transition metal surfaces such as Fe or Ru: atomic nitrogen is adsorbed in a hollow site, NH_2 is adsorbed in a bridge site, and NH_3 is bound on-top.[72,76,78,79] In addition, the mechanism of ammonia synthesis with these catalysts (LaRuSi, Fe, and Ru) is a dissociative mechanism, but the activation barrier for the dissociation of N_2 is much lower on LaRuSi (0.84 eV) than on Ru (1.30 eV)[72] and Fe (1.27 eV).[78]

The inferior catalytic performances of CaRuSi compared to LaRuSi are attributed to the weak adsorption of nitrogen on the Ca-terminated surface and to the rather high (larger than 1.35 eV) activation energies of N + H → NH, NH + H → NH_2, and NH_2 + H → NH_3. The nitrogen dissociation barrier has been calculated to be similar on LaRuSi and CaRuSi, which is inconsistent with the general idea that a stronger surface nitrogen bond is accompanied by a low nitrogen dissociation barrier.[80] Does the electride character of LaRuSi play a role in the synthesis of ammonia on this catalyst? Since the bulk electride character disappears when the bulk $[R]_4$ sites are occupied by hydrogen atoms (Figure S1b), and given that the reaction energy profile is quiet similar with or without absorbed H atoms, it suggests that the bulk electride character does not impact the catalytic properties of the surface.

The proposed mechanism points to the role of surface La atoms in the catalytic properties of LaRuSi, which contribute in the specific electronic and atomic surface structure. This conclusion may be valid at the surface of other electrides, such as LaCoSi. This work emphasizes that active sites are not necessarily transition metal atoms. It presents deep insights into the reaction path and thus may help to provide guidelines for designing intermetallic catalysts with optimal performance.

ASSOCIATED CONTENT

Supporting Information

The Supporting Information is available free of charge at https://pubs.acs.org/doi/10.1021/acs.jpcc.1c08725.

Bulk parameters and bulk thermodynamic properties; discussion of the electride character including partial electron densities of bulk compounds; surface energies, surface electron charge densities, diagram of projected density of states for slabs, charge density discussion with partial electron densities diagram; adsorption energies and geometries, COHP analysis; reaction paths; hydrogen absorption diagram (PDF)

AUTHOR INFORMATION

Corresponding Author

Émilie Gaudry − *Université de Lorraine, CNRS, Institut Jean Lamour, F-54011 Nancy, France;* orcid.org/0000-0001-6546-8323; Email: emilie.gaudry@univ-lorraine.fr

Authors

Florian Brix − *Université de Lorraine, CNRS, Institut Jean Lamour, F-54011 Nancy, France*

Gilles Frapper − *Applied Quantum Chemistry Group, E4 Team, IC2MP UMR 7285, Université de Poitiers - CNRS, 86073 Poitiers, Cedex 9, France*

Notes

The authors declare no competing financial interest.

ACKNOWLEDGMENTS

This work is supported by the European Integrated Center for the Development of New Metallic Alloys and Compounds. We acknowledge financial support through the COMETE project (COnception in silico de Matériaux pour l'EnvironnemenT et l'Énergie) cofunded by the European Union under the program FEDER-FSE Lorraine et Massif des Vosges 2014-2020. This work was granted access to the HPC resources of TGCC, CINES, and IDRIS under the allocation 99 642 attributed by GENCI (Grand Equipement National de Calcul Intensif). High Performance Computing resources were also partially provided by the EXPLOR centre hosted by the University de Lorraine (project 2017M4XXX0108). G.F. thanks the Région Nouvelle Aquitaine and CNRS.

REFERENCES

(1) Liu, H. Z. Ammonia Synthesis Catalyst 100 Years: Practice, Enlightenment and Challenge. *Chin. J. Catal.* **2014**, *35*, 1619−1640.

(2) Saadatjou, N.; Jafari, A.; Sahebdelfar, S. Ruthenium Nanocatalysts for Ammonia Synthesis: A Review. *Chem. Eng. Commun.* **2015**, *202*, 420−448.

(3) Frink, C. R.; Waggoner, P.; Ausubel, J. Nitrogen Fertilizer: Retrospect and Prospect. *Proc. Natl. Acad. Sci. U. S. A.* **1999**, *96*, 1175−1180.

(4) Smith, C.; Hill, A. K.; Torrente-Murciano, L. Current and Future Role of Haber−Bosch Ammonia in a Carbon-Free Energy Landscape. *Energy Environ. Sci.* **2020**, *13*, 331−344.

(5) Guo, J.; Chen, P. Catalyst: NH_3 as an Energy Carrier. *Chem.* **2017**, *3*, 709−712.

(6) Giddey, S.; Badwal, S. P. S.; Munnings, C.; Dolan, M. Ammonia as a Renewable Energy Transportation Media. *ACS Sustainable Chem. Eng.* **2017**, *5*, 10231−10239.

(7) Vanderzee, C. E.; King, D. L. The Enthalpies of Solution and Formation of Ammonia. *J. Chem. Thermodyn.* **1972**, *4*, 675−683.

(8) Larson, A. T.; Dodge, R. L. The Ammonia Equilibrium. *J. Am. Chem. Soc.* **1923**, *45*, 2918−2930.

(9) Ertl, G. Surface Science and Catalysis—Studies on the Mechanism of Ammonia Synthesis: The P. H. Emmett Award Address. *Catal. Rev.: Sci. Eng.* **1980**, *21*, 201−223.

(10) Garden, A. L.; Skulason, E. The Mechanism of Industrial Ammonia Synthesis Revisited: Calculations of the Role of the Associative Mechanism. *J. Phys. Chem. C* **2015**, *119*, 26554−26559.
(11) Jacobsen, C.; Dahl, S.; Clausen, B.; Bahn, S.; Logadottir, A.; Norskov, J. Catalyst Design by Interpolation in the Periodic Table: Bimetallic Ammonia Synthesis Catalyst. *J. Am. Chem. Soc.* **2001**, *123*, 8404−8405.
(12) Schlögl, R. Catalytic Synthesis of Ammonia - A Never-Ending Story? *Angew. Chem., Int. Ed.* **2003**, *42*, 2004−2008.
(13) Kitano, M.; Kanbara, S.; Inoue, Y.; Kuganathan, N.; Sushko, P. V.; Yokoyama, T.; Hara, M.; Hosono, H. Electride Support Boosts Nitrogen Dissociation Over Ruthenium Catalyst and Shifts the Bottleneck in Ammonia Synthesis. *Nat. Commun.* **2015**, *6*, 6731.
(14) Hinrichsen, O.; Rosowski, F.; Hornung, A.; Muhler, M.; Ertl, G. The Kinetics of Ammonia Synthesis over Ru-Based Catalysts. The Dissociative Chemisorption and Associative Desorption of N_2. *J. Catal.* **1997**, *165*, 33−44.
(15) Niwa, Y.; Aika, K.-I. The Effect of Lanthanide Oxides as a Support for Ruthenium Catalysts in Ammonia Synthesis. *J. Catal.* **1996**, *162*, 138−142.
(16) Kitano, M.; Inoue, Y.; Ishikawa, H.; Yamagata, K.; Nakao, T.; Tada, T.; Matsuishi, S.; Yokoyama, T.; Hara, M.; Hosono, H. Essential Role of Hydride Ion in Ruthenium-Based Ammonia Synthesis Catalysts. *Chem. Sci.* **2016**, *7*, 4036−4043.
(17) Vojvodic, A.; Medford, A. J.; Studt, F.; Abild-Pedersen, F.; Suvra-Khan, T.; Bligaard, T.; Norskov, J. K. Exploring the limits: a Low-Pressure, Low-Temperature Haber-Bosch process. *Chem. Phys. Lett.* **2014**, *598*, 108−112.
(18) Wang, Q.; Guo, J.; Chen, P. Recent Progress Towards Mild-Condition Ammonia Synthesis. *J. Energy Chem.* **2019**, *36*, 25−36.
(19) Zhang, S.; Zhao, Y.; Shi, R.; Waterhouse, G. I.; Zhang, T. Photocatalytic Ammonia Synthesis: Recent Progress and Future. *EnergyChem.* **2019**, *1*, 100013.
(20) Han, Q.; Jiao, H.; Xiong, L.; Tang, J. Progress and Challenges in Photocatalytic Ammonia Synthesis. *Mater. Adv.* **2021**, *2*, 564−581.
(21) Hu, L.; Xing, Z.; Feng, X. Understanding the Electrocatalytic Interface for Ambient Ammonia Synthesis. *ACS Energy Letters* **2020**, *5*, 430−436.
(22) Martirez, J. M. P.; Carter, E. A. Prediction of a Low-Temperature N_2 Dissociation Catalyst Exploiting Near-IR-to-Visible Light Nanoplasmonics. *Sci. Adv.* **2017**, *3*, No. eaao4710.
(23) Inoue, Y.; Kitano, M.; Kishida, K.; Abe, H.; Niwa, Y.; Sasase, M.; Fujita, Y.; Ishikawa, H.; Yokoyama, T.; Hara, M.; Hosono, H. Efficient and Stable Ammonia Synthesis by Self-Organized Flat Ru Nanoparticles on Calcium Amide. *ACS Catal.* **2016**, *6*, 7577−7584.
(24) Ogawa, T.; Kobayashi, Y.; Mizoguchi, H.; Kitano, M.; Abe, H.; Tada, T.; Toda, Y.; Niwa, Y.; Hosono, H. High Electron Density on Ru in Intermetallic YRu_2: The Application to Catalyst for Ammonia Synthesis. *J. Phys. Chem. C* **2018**, *122*, 10468−10475.
(25) Wu, J.; Gong, Y.; Inoshita, T.; Fredrickson, D. C.; Wang, J.; Lu, Y.; Kitano, M.; Hosono, H. Tiered Electron Anions in Multiple Voids of LaScSi and Their Applications to Ammonia Synthesis. *Adv. Matter.* **2017**, *29*, 1700924.
(26) Ooya, K.; Li, J.; Fukui, K.; Iimura, S.; Nakao, T.; Ogasawara, K.; Sasase, M.; Abe, H.; Niwa, Y.; Kitano, M.; Hosono, H. Ammonia Synthesis: Ruthenium Catalysts Promoted by Lanthanide Oxy-hydrides with High Hydride-Ion Mobility for Low-Temperature Ammonia Synthesis. *Adv. Energy Mater.* **2021**, *11*, 2170018.
(27) Li, J.; Wu, J.; Wang, H.; Lu, Y.; Ye, T.; Sasase, M.; Wu, X.; Kitano, M.; Inoshita, T.; Hosono, H. Acid-Durable Electride With Layered Ruthenium for Ammonia Synthesis: Boosting the Activity via Selective Etching. *Chem. Sci.* **2019**, *10*, 5712−5718.
(28) Lee, K.; Kim, S. W.; Toda, Y.; Matsuishi, S.; Hosono, H. Dicalcium Nitride as a Two-Dimensional Electride With An Anionic Electron Layer. *Nature* **2013**, *494*, 336−340.
(29) Gong, Y.; Wu, J.; Kitano, M.; Wang, J.; Ye, T.-N.; Li, J.; Kobayashi, Y.; Kishida, K.; Abe, H.; Niwa, Y.; Yang, H.; Tada, T.; Hosono, H. Ternary Intermetallic LaCoSi as a Catalyst for N_2 Activation. *Nat. Catal.* **2018**, *1*, 178−185.
(30) Wu, J.; Li, J.; Gong, Y.; Kitano, M.; Inoshita, T.; Hosono, H. Intermetallic Electride Catalyst as a Platform for Ammonia Synthesis. *Angew.Chem. Int. Ed.* **2019**, *58*, 825−829.
(31) Hosono, H.; Kitano, M. Advances in Materials and Applications of Inorganic Electrides. *Chem. Rev.* **2021**, *121*, 3121−3185.
(32) Wang, Y.; Kattel, S.; Gao, W.; Li, K.; Liu, P.; Chen, J. G.; Wang, H. Exploring the Ternary Interactions in $Cu−ZnO−ZrO_2$ Catalysts for Efficient CO_2 Hydrogenation to Methanol. *Nat. Commun.* **2019**, *10*, 1166.
(33) Harris, J.; Kasemo, B. On Precursor Mechanisms for Surface Reactions. *Surf. Sci. Letters* **1981**, *105*, L281.
(34) Park, J. Y.; Kim, S. M.; Lee, H.; Nedrygailov, I. I. Hot-Electron-Mediated Surface Chemistry: Toward Electronic Control of Catalytic Activity. *Acc. Chem. Res.* **2015**, *48*, 2475−2483.
(35) Wintterlin, J.; Schuster, R.; Ertl, G. Existence of a "Hot" Atom Mechanism for the Dissociation of O_2 on Pt(111). *Phys. Rev. Lett.* **1996**, *77*, 123−126.
(36) Sun, Y.; Chen, Y.; Zhang, X.; He, Y.; Qiu, Z.; Zheng, W.; Wang, F.; Jiao, H.; Yang, Y.; Li, Y.; Wen, X.-D. The Facile Dissociation of Carbon-Oxygen bonds in CO_2 and CO on the Surface of $LaCoSiH_x$ Intermetallic Compound. *Angew. Chem., Int. Ed.* **2021**, *60*, 25538.
(37) Wu, P.; Yang, B. Intermetallic PdIn Catalyst for CO_2 Hydrogenation to Methanol: Mechanistic Studies with a Combined DFT and Microkinetic Modeling Method. *Catal. Sci. Technol.* **2019**, *9*, 6102.
(38) Tran, R.; Xu, Z.; Radhakrishnan, B.; Winston, D.; Sun, W.; Persson, K.; Ping-Ong, S. Surface Energies of Elemental Crystals. *Sci. Data* **2016**, *3*, 160080.
(39) Kresse, G.; Hafner, J. Ab Initio Molecular Dynamics for Liquid Metals. *Phys. Rev. B* **1993**, *47*, 558−561.
(40) Kresse, G.; Furthmüller, J. Efficient Iterative Schemes for Ab Initio Total-Energy Calculations Using A Plane-Wave Basis Set. *Phys. Rev. B* **1996**, *54*, 11169−11186.
(41) Kresse, G.; Furthmüller, J. Efficiency of Ab-Initio Total Energy Calculations For Metals and Semiconductors Using a Plane Wave Basis Set. *Comput. Mater. Sci.* **1996**, *6*, 15−50.
(42) Blochl, P. E. Projector Augmented-Wave Method. *Phys. Rev. B* **1994**, *50*, 17953−17979.
(43) Kresse, G.; Joubert, D. From Ultrasoft Pseudopotentials To the Projector Augmented-Wave Method. *Phys. Rev. B* **1999**, *59*, 1758−1775.
(44) Grimme, S.; Ehrlich, S.; Goerigk, L. Effect of The Damping Function in Dispersion Corrected Density Functional Theory. *J. Comput. Chem.* **2011**, *32*, 1456.
(45) Sanville, E.; Kenny, S. D.; Smith, R.; Henkelman, G. An Improved Grid-Based Algorithm for Bader Charge Allocation. *J. Comput. Chem.* **2007**, *28*, 899−908.
(46) Bader, R. F. W. Atoms in Molecules: A Quantum Theory. *Chem. Rev.* **1991**, *91*, 893.
(47) Henkelman, G.; Arnaldsson, A.; Jónsson, H. A Fast and Robust Algorithm for Bader Decomposition of Charge Density. *Comput. Mater. Sci.* **2006**, *36*, 354−360.
(48) Mills, G.; Jonsson, H.; Schenter, G. K. Reversible Work Transition State Theory: Application to Dissociative Adsorption of Hydrogen. *Surf. Sci.* **1995**, *324*, 305.
(49) Jónsson, H.; Mills, G.; Jacobsen, K. W. Nudged Elastic Band Method for Finding Minimum Energy Paths of Transitions. In *Classical and Quantum Dynamics in Condensed Phase Simulations*; Berne, B. J., Ciccotti, G., Coker, D. F.. Eds.; World Scientific: New-York, 1998; Chapter 16, p 385.
(50) Henkelman, G.; Uberuaga, B. P.; Jónsson, H. A Climbing Image Nudged Elastic Band Method for Finding Saddle Points and Minimum Energy Paths. *J. Chem. Phys.* **2000**, *113*, 9901.
(51) Henkelman, G.; Jónsson, H. Improved Tangent Estimate in The Nudged Elastic Band Method for Finding Minimum Energy Paths and Saddle Points. *J. Chem. Phys.* **2000**, *113*, 9978.
(52) Heyden, A.; Bell, A. T.; Keil, F. J. Efficient Methods For Finding Transition States In Chemical Reactions: Comparison of

Improved Dimer Method and Partitioned Rational Function Optimization Method. *J. Chem. Phys.* **2005**, *123*, 224101.
(53) Henkelman, G.; Jonsson, H. A Dimer Method for Finding Saddle Points on High Dimensional Potential Surfaces Using Only First Derivatives. *J. Chem. Phys.* **1999**, *111*, 7010−7022.
(54) Tang, W.; Sanville, E.; Henkelman, G. A Grid-Based Bader Analysis Algorithm without Lattice Bias. *J. Phys.: Condens. Matter* **2009**, *21*, 084204.
(55) Yu, M.; Trinkle, D. R. Accurate and Efficient Algorithm for Bader Charge Integration. *J. Chem. Phys.* **2011**, *134*, 064111.
(56) Dronskowski, R.; Blöchl, P. E. The Original COHP Definition. *J. Phys. Chem.* **1993**, *97*, 8617−8624.
(57) Deringer, V. L.; Tchougréeff, A. L.; Dronskowski, R. Crystal Orbital Hamilton Population (COHP) Analysis as Projected from Plane-Wave Basis Sets. *J. Phys. Chem. A* **2011**, *115*, 5461−5466.
(58) Maintz, S.; Deringer, V. L.; Tchougréeff, A. L.; Dronskowski, R. The Mathematical Apparatus and the Framework on which LOBSTER is Built. *J. Comput. Chem.* **2013**, *34*, 2557−2567.
(59) Maintz, S.; Deringer, V. L.; Tchougreeff, A. L.; Dronskowski, R. LOBSTER: A Tool to Extract Chemical Bonding from Plane-Wave Based DFT. *J. Comput. Chem.* **2016**, *37*, 1030−1035.
(60) Dahl, S.; Logadottir, A.; Egeberg, R. C.; Larsen, J. H.; Chorkendorff, I.; Törnqvist, E.; Norskov, J. K. Role of Steps in N_2 Activation on Ru(0001). *Phys. Rev. Lett.* **1999**, *83*, 1814.
(61) Dahl, S.; Tornqvist, E.; Chorkendorff, I. Dissociative Adsorption of N on Ru(0001): a Surface Reaction Totally Dominated by Steps. *J. Catal.* **2000**, *192*, 381−390.
(62) Jacobsen, C. J.; Dahl, S.; Hansen, P.; Tornqvist, E.; Jensen, L.; Topsoe, H.; Prip, D. V.; Moenshaug, P.; Chorkendorff, I. Structure Sensitivity of Supported Ruthenium Catalysts for Ammonia Synthesis. *J. Mol. Catal. A: Chem.* **2000**, *163*, 19−26.
(63) Boudart, M. Kinetics and Mechanism of Ammonia Synthesis. *Catal. Rev.: Sci. Eng.* **1981**, *23*, 1−15.
(64) Aika, K.-I. Role of Alkali Promoter in Ammonia Synthesis over Ruthenium Catalysts: Effect on Reaction Mechanism. *Catal. Today* **2017**, *286*, 14−20.
(65) Zhao, P.; He, Y.; Cao, D.-B.; Wen, X.; Xiang, H.; Li, Y.-W.; Wanga, J.; Jiao, H. High Coverage Adsorption and Co-Adsorption of CO and H2 On Ru(0001) from DFT and Thermodynamics. *Phys. Chem. Chem. Phys.* **2015**, *17*, 19446.
(66) Mamun, O.; Winther, K. T.; Boes, J. R.; Bligaard, T. High-Throughput Calculations of Catalytic Properties of Bimetallic Alloy Surfaces. *Sci. Data* **2019**, *6*, 76.
(67) Ferrin, P.; Kandoi, S.; Nilekar, A. U.; Mavrikakis, M. Hydrogen Adsorption, Absorption and Diffusion on and in Transition Metal Surfaces: A DFT Study. *Surf. Sci.* **2012**, *606*, 679.
(68) Degtyareva, O.; Canales, M. M.; Bergara, A.; Chen, X.-J.; Song, Y.; Struzhkin, V. V.; Mao, H.-K.; Hemley, R. J. Crystal Structure of SiH_4 at High Pressure. *Phys. Rev. B* **2007**, *76*, 064123.
(69) Chan, J. R.; Lambie, S. G.; Trodahl, H. J.; Lefebvre, D.; Le Ster, M.; Shaib, A.; Ullstad, F.; Brown, S. A.; Ruck, B. J.; Garden, A. L.; Natali, F. Facile Dissociation of Molecular Nitrogen Using Lanthanide Surfaces: Towards Ambient Temperature Ammonia Synthesis. *Phys. Rev. Mater.* **2020**, *4*, 115003.
(70) Cheng, J.; Hu, P. Theory of the Kinetics of Chemical Potentials in Heterogeneous Catalysis. *Angew. Chem., Int. Ed.* **2011**, *50*, 7650−7654.
(71) Bligaard, T.; Norskov, J. K.; Dahl, S.; Matthiesen, J.; Christensen, C. H.; Sehested, J. The Brønsted-Evans-Polanyi Relation and the Volcano Curve in Heterogeneous Catalysis. *J. Catal.* **2004**, *224*, 206.
(72) Logadottir, A.; Norskov, J. Ammonia Synthesis over a Ru(0001) Surface Studied By Density Functional Calculations. *J. Catal.* **2003**, *220*, 273−279.
(73) Ishikawa, A.; Doi, T.; Nakai, H. Catalytic Performance of Ru, Os, and Rh Nanoparticles for Ammonia Synthesis: a Density Functional Theory Analysis. *J. Catal.* **2018**, *357*, 213−222.
(74) Wang, T.; Abild-Pedersen, F. Achieving Industrial Ammonia Synthesis Rates at Near Ambient Condition through Modified Scaling Relations on a Confined Dual Site. *Proc. Natl. Acad. Sci.* **2021**, *118*, No. e2106527118.
(75) Rod, T. H.; Logadottir, A.; Norskov, J. K. J. Ammonia Synthesis at Low Temperatures. *Chem. Phys.* **2000**, *112*, 5343.
(76) Zeinalipour-Yazdi, C. D.; Hargreaves, J. S. J.; Laassiri, S.; Catlow, C. R. A. A Comparative Analysis of the Mechanisms of Ammonia Synthesis on Various Catalysts Using Density Functional Theory. *R. Soc. Open Sci.* **2021**, *8*, 210952.
(77) Hodge, K. L.; Goldberger, J. E. Transition Metal-Free Alkyne Hydrogenation Catalysis with $BaGa_2$, a Hydrogen Absorbing Layered Zintl Phase. *J. Am. Chem. Soc.* **2019**, *141*, 19969−19972.
(78) Qian, J.; An, Q.; Fortunelli, A.; Nielsen, R.; Goddard, W. Reaction Mechanism and Kinetics for Ammonia Synthesis on the Fe(111) Surface. *J. Am. Chem. Soc.* **2018**, *140*, 6288−6297.
(79) Fuller, J.; Fortunelli, A.; Goddard, W.; An, Q. Reaction Mechanism And Kinetics For Ammonia Synthesis On The Fe(211) reconstructed surface. *Phys. Chem. Chem. Phys.* **2019**, *21*, 11444−11454.
(80) Norskov, J. K.; Stoltze, P. Theoretical Aspects of Surface Reactions. *Surf. Sci.* **1987**, *189190*, 91.